Determining the Optimum Temperature Path Versus the Catalyst Working Time in a Trickle Bed Diesel Hydrodesulfurization Reactor

H. Reza Homayonfar,[a] H. Ale Ebrahim,[a] and M. J. Azarhoosh[b,*]

[a]Department of Chemical Engineering, Amirkabir University of Technology (Tehran Polytechnic), Tehran, Iran

[b]Department of Chemical Engineering, Faculty of Engineering, Urmia University, Urmia, Iran

This study consists of four main parts. First, a heterogeneous reactor model was developed to simulate a diesel hydrodesulfurization (HDS) reactor with catalyst deactivation. Second, operating conditions were investigated. Third, the simulation results from the first part were modeled using the response surface method and artificial neural networks (ANNs) to shorten the temperature path optimization time. Among the different modeling methods, the feed-forward ANN method employing the Bayesian Regularization (BR) training method with 10 neurons in the hidden layer demonstrated the highest accuracy. Finally, the temperature path of the trickle bed reactor was optimized. A three-dimensional curve depicting sulfur output content versus temperature and catalyst operation time was plotted using the most effective ANN approach as a fitness function. When the sulfur content met the Euro-6 requirement, the temperature path versus catalyst working period was optimized.

Keywords

hydrodesulfurization, trickle bed reactor, catalyst deactivation, reactor simulation, artificial neural networks

Introduction

Hydrodesulfurization

Environmental regulations aim to reduce sulfur dioxide, nitrogen oxides, aromatics, and soot particles from industrial and refinery operations to comply with legal gas emission standards. The hydrodesulfurization (HDS) process is one of the most effective methods used in refineries for sulfur removal[1]. Evolving environmental regulations will impact HDS unit operations, including hydrogen consumption, light hydrocarbon yield, liquid purity, and temperature variations in HDS reactors[2].

Catalyst deactivation, characterized by the loss of catalytic activity and decreased selectivity, is a primary concern in HDS reactor performance. This leads to reduced production time and increased sulfur content[3]. Causes of catalyst deactivation include organized segregation, sintering molybdenum disulfide (MoS_2) catalysts, poisoning by nitrogen, metal deposition, and coking[4]. The oil industry commonly utilizes two-phase fixed-bed catalytic reactors and trickle bed reactors (TBRs) in the HDS process[5].

TBRs are employed in various applications, such as hydrodesulfurization, hydrocracking, and hydropurification. These reactors operate at high pressures to enhance gas-phase solubility, optimize heat transfer, and dissolve otherwise insoluble components in the reaction medium[6,7]. Designing TBRs involves considering mass transfer and chemical reactions within each phase[8]. Given that HDS feed consists of a gas and liquid mixture, catalyst deactivation should be factored into reactor modeling and optimization[9].

Hydrotreating catalyst deactivation kinetic model

HDS catalyst deactivation occurs in three stages of. During the first hours of the process, asphaltene molecules typically form coke at high temperatures. In the second stage, metals gradually cover the catalyst's surface over extended periods. Finally, at the end of the catalyst's life, both metals and coke deposit within its pores. In dynamic simulations, these stages result in an S-shaped curve for catalyst life[10]. Severe operating conditions, such as high reaction temperatures, low H_2-to-oil ratios, or feedstock with an excessive compound content, can accelerate hydrotreating catalyst deactivation, leading to coke and metal deposition[11].

*Corresponding author: Mohammad Javad Azarhoosh
E-mail: mj.azarhoosh@urmia.ac.ir, Tel: +98 44 3194 2893

Koseoglu and Al-Sobhi conducted a kinetic study on a heavy gas oil hydrotreating (HDT) unit to determine the catalyst deactivation rate. They concluded that the reactor temperature must be increased by 1.3 °C monthly to maintain standard product quality. Conversely, Torres-Mancera et al.[12], in their analysis of a bench-scale continuous stirred tank reactor, noted that increasing the operating temperature accelerated the rate of catalyst deactivation due to the higher refractory coke-to-aromaticity ratio at elevated operating temperatures. High operating temperatures are beneficial for removing feed metals since the reactor operates at higher temperatures than the HDS reaction. Jiang et al.[8] developed a kinetic model for the HDS and hydrodemetallation (HDM) reactions of residue oil feed. They determined kinetic parameters such as reaction order, activation energy, reaction rate constant, and activity coefficient. A decrease in catalyst activity due to metal deposition over time was observed, indicating that catalyst activity coefficient parameters linearly depend on metal deposition. They also demonstrated that pore diffusion affected the reaction rate during metal deposition.

Marafi et al.[13] conducted a comparative study on the deactivation of industrial HDT catalysts using Mo/Al_2O_3, $Ni-Mo/Al_2O_3$, $Ni-MoP/Al_2O_3$ in three commercial atmospheric residue reactors. They found that coke rapidly accumulated on the catalyst during the initial step of HDT, and the order of coke buildup was HDS < HDM < HDS/HDN (hydrodenitrogenation).

Soltanali et al.[14] modified the commercial $NiMo/Al_2O_3$ catalyst by adding phosphorus and boron for the diesel fuel HDT process. The modified catalyst produced 20 ppm sulfur and 7 ppm nitrogen content at the reactor outlet for HDS and HDN reactions. Under identical operating conditions, the unmodified catalyst produced 86 ppm of sulfur and 12 ppm of nitrogen.

Leandro da Rocha Novaes et al.[15] investigated the effect of feed properties on product specifications due to deactivation phenomena related to oil fraction composition. They observed that oil feed containing heavy compounds expedited catalyst deactivation, for, and they implemented harsh conditions such as increased temperatures and reduced H_2/oil ratios to enhance the aromatic compound concentrations.

For HDS, controlling temperature is critical for maintaining product quality and managing catalyst deactivation, as highlighted in previous studies. While earlier research has examined the effect of temperature changes on product quality, this study focuses on optimizing the temperature during the process with catalyst deactivation, following reactor simulation.

Simulation of hydrotreating reactors

Mederos et al. developed a one-dimensional dynamic heterogeneous TBR model for catalytic HDT of oil fractions. This model includes HDS, HDN, hydrodearomatization (HDA), olefin hydrogenation, and moderate hydrocracking, all of which are essential processes in the HDT process. The model simulates temperature, partial pressure, and concentration profiles[2].

To replicate the bench-scale HDT of a vegetable oil reactor, Alexis Tirado et al. developed a dynamic non-isothermal TBR model. In this process, the top of the catalytic bed experiences significant temperature increases, substantially raising the inlet reactor temperature. This temperature rise is primarily due to triglyceride depropanation[16].

Neto et al. used a plug-flow three-phase TBR model to calculate the performance of an industrial diesel hydrotreating reactor, which considers most HDT reactions, gas-liquid and liquid-solid mass transfer, and the influence of catalytic deactivation in the industrial HDT reactor model[17].

Al-Jamimi et al. presented a multi-objective optimization of diesel fuel HDS using distillation with a side reactor. By optimizing the three opposing objectives, they identified the operating conditions. Their results indicated that separation schemes for distillation with side reactors may be more effective for the HDS process than reactive distillation[18].

Srinivas et al. investigated the ideal conditions for reducing sulfur content and increasing total aromatics conversion at the TBR outlet. They first used a simple genetic algorithm (GA) to solve two independent optimization problems: reducing sulfur concentration at the outflow and increasing aromatic conversion. They then used the non-dominated sorting genetic algorithm-II (NSGA-II) to solve a multi-objective optimization problem planned using two objective functions at the same time[19].

Goals of this study

According to the Euro-6 environmental standard, diesel fuel can have a maximum sulfur content of 10 ppm[20]. This study aimed to determine the optimum operating temperature path concerning the catalyst working time, determined by the sulfur content in the diesel fuel output from the HDS reactor, in compliance with the Euro-6 standard. To achieve this goal, the study followed four general steps:

Step 1) Hydrotreating trickle bed reactor dynamic simulation

This study applied a heterogeneous reactor model based on the two-film theory to an HDS TBR

simulation with catalyst deactivation. The catalyst activity model employed various deactivation functions.

Step 2) Evaluation of operating parameters

The impact of operating conditions such as temperature, pressure, space velocity, and stream time was investigated.

Step 3) Modeling dynamic simulation results using response surface methodology and artificial neural networks

Dynamic simulation of the HDS reactor was coded in MATLAB R2021a software. The program runs in approximately 15 minutes on a system with the following specifications (Processor: Intel(R) Core(TM) i7-10510U CPU @ 1.80GHz, 2.30GHz, RAM 8.00GB). Using dynamic simulation as a fitness function for temperature path optimization would be time-prohibitive. Therefore, response surface methodology (RSM) and artificial neural network (ANN) methods were used to model the dynamic simulation results and reduce the time required for temperature path optimization. The model with the most accurate performance was used as the fitness function in optimization.

Step 4) Finding the optimal temperature path versus time

As previously mentioned, most articles do not discuss HDS catalyst deactivation; however, in industrial reactors with heavy feeds, the catalyst activity gradually decreases over time[21]. This study plotted a three-dimensional curve of sulfur output content versus temperature and catalyst operating time using the results from the most accurate modeling method. Consequently, the temperature path and the catalyst's working time were optimized to meet the Euro-6 sulfur content standard.

Computation methods

Reactor simulation

Kinetic model

The kinetic equation of the HDS reaction is described by Langmuir-Hinshelwood relation. In HDN, non-basic nitrogen (N_{NB}) is initially converted to basic nitrogen (N_B), which then undergoes further reaction to eliminate the nitrogen from the molecule. Aromatic saturation is assumed by a reversible reaction. The kinetic parameters for HDS, HDN, and HAD reactions were assumed to be similar to those in our previous work[22].

Reactor model

This study employed a one-dimensional heterogeneous reactor model to simulate the TBR for the HDS of diesel fuel[23].

The model is based on the following assumptions:

1. Mass transfer is based on the two-film theory.
2. The liquid and gas phases behave as plug flow
3. Energy balance is ignored at the bench scale.
4. Liquid evaporation along the catalytic bed is negligible.
5. The effectiveness factor approximates the resistance to intra-particle mass transfer.
6. Chemical reactions occur only on the catalyst's solid surface.
7. Catalyst activity changes with time and temperature.
8. Catalyst particles are thoroughly wetted in the liquid phase.

The mass balance equations for the compounds present in the gas phase in the catalyst bed are expressed as follows[23]:

$$\frac{u_G}{RT}\frac{dp_i^G}{dz} + k_i^G a_L \left(\frac{p_i^G}{H_i} - C_i^L \right) = 0, \quad (1)$$

$$i = H_2 \text{ and } H_2S$$

The following is the mass balance equation for gaseous components in the liquid phase[23]:

$$u_L \frac{dC_i^L}{dz} - k_i^L a_L \left(\frac{p_i^G}{H_i} - C_i^L \right) + k_i^s a_s \left(C_i^L - C_i^S \right) = 0, \quad (2)$$

$$i = H_2 \text{ and } H_2S$$

For liquid components, mass balance equations are described as follows[23]:

$$u_L \frac{dC_i^L}{dz} + k_i^s a_s \left(C_i^L - C_i^S \right) = 0, \quad (3)$$

$$i = S, \ N_B, \ N_{NB} \text{ and } A$$

The mass balance equations at the surface of the catalyst are as follows[23]:

$$k_i^s a_s \left(C_i^L - C_i^S \right) = -\rho_B \eta_j r_j \gamma, \quad (4)$$

$$i = H_2, \ H_2S, \ S, \ N_B, \ N_{NB}, \text{ and } A$$

The effectiveness factors can be obtained from the following equation[24]:

$$\eta_j = \frac{-r_{j, \text{ act}}}{-r_{j, \text{ surface}}} = \frac{3}{R_p^3} \frac{\int r^2 \left(-r_j \right) dr}{-r_{j, \text{ surface}}} \quad (5)$$

The mass balance equation within the pores of the catalyst pellet is as follows[25]:

$$\frac{d^2 C_i^s}{dr^2} + \frac{2}{r}\left(\frac{dC_i^s}{dr}\right) - r_j = 0, \tag{6}$$

$$i = H_2,\ H_2S,\ S,\ N_B,\ N_{NB},\ \text{and A}$$

Catalyst activity functions

Catalyst deactivation functions are assumed as various equations. Firstly, for validation with literature data, the following functions were considered[26,27]:

$$\gamma_1 = t^{(-0.16)} \tag{7}$$

$$\gamma_2 = e^{\left(\frac{-t}{5000}\right)} \tag{8}$$

Another function was considered as activity versus time[27,29]:

$$\gamma_3 = \left[1 - 0.00306 \cdot t^{0.5}\right]^{4.3} \tag{9}$$

$$\gamma_4 = \varphi_s + (1 - \varphi_s)e^{-0.0001 \cdot (0.465 \cdot t - 10000)} \tag{10}$$

Finally, the effects of time and temperature were inserted into the catalyst deactivation function[30]:

$$\gamma_5 = 10 \cdot e^{(x - y + z)} \tag{11}$$

$$x = \ln\left(1 + 1.89 \cdot e^{(\alpha_1 - \alpha_2)\cdot t}\right) \tag{12}$$

$$y = 1.29 \cdot \left(0.32314 + (\alpha_3 \cdot t \cdot \alpha_4)\right) + 2.5 \tag{13}$$

$$z = 0.09 \cdot \left[\ln\left(\frac{1}{\varphi_s + \dfrac{(\varphi_s - 0.3)}{1 - t/t_\infty}}\right)\right] \tag{14}$$

where:

$$\alpha_1 = 9 \cdot 10^{-3} \tag{15}$$

$$\alpha_2 = 1.22 \cdot 10^{10} \cdot e^{\left(\frac{175 \cdot T}{1000 \cdot R}\right)} \tag{16}$$

$$\alpha_3 = 10^{-19} \tag{17}$$

$$\alpha_4 = 1.22 \cdot 10^{10} \cdot e^{\left(\frac{175 \cdot T}{1000 \cdot R}\right)} \tag{18}$$

$$t_\infty = 90000 \tag{19}$$

Numerical solution

For the numerical solution of the set of differential equations in the axial direction of the reactor as well as around the reaction-diffusion equations within the catalyst disk, the boundary, and initial conditions were defined as follows:

Reactor:

$$\text{At } z = 0:\ p_{H_2}^G = \left(p_{H_2}^G\right)_0 \tag{20}$$

$$p_{H_2S}^G = 0 \tag{21}$$

$$C_i^L = \left(C_i^L\right)_0,\ i = H_2,\ S,\ N_B,\ N_{NB} \text{ and A} \tag{22}$$

$$C_i^L = 0,\ i = H_2S \tag{23}$$

$$C_i^S = 0,\ i = H_2,\ H_2S,\ S,\ N_B,\ N_{NB} \text{ and A} \tag{24}$$

$$T = T_0 \tag{25}$$

Catalyst:

$$\text{At } r = 0:\ \frac{dC_i^s}{dr} = 0 \tag{26}$$

$$\text{At } r = R_p:\ C_i^s = C_i^L,\ i = H_2,\ H_2S,\ S,\ N_B,\ N_{NB} \text{ and A} \tag{27}$$

Differential equations of the reactor were treated as initial value problems (IVPs), and diffusion equations were treated as boundary value problems (BVPs).

The differential equations were included in eight ordinary differential equations (ODEs) for the description of axial changes of compounds in the liquid phase, which were solved simultaneously with the BVP equations.

The Runge-Kutta 4 method was used to solve the IVP equations, and the bvp4c MATLAB function was used for the BVP equations.

Property prediction

The model requires dependable correlations to calculate mass transfer coefficients for gas-liquid and liquid-solid interfaces, gas solubilities, and specifications for products and feedstock. Table 1 shows the corresponding correlations[23].

Modeling methods

Response surface modeling

Response surface methodology (RSM) is a mathematical technique that establishes the relationship between a response variable and independent variables. Introduced by Box and Wilson in 1951, RSM is still utilized as an experimental design tool today.

This strategy aids in analyzing experiments where multiple independent variables influence one or more response variables, with the goal of optimizing the response. The relationship obtained from RSM is expressed as follows[31,32]:

$$Y = \alpha_0 + \sum_{i=1}^{n} X_i + \sum_{i=1}^{n}\sum_{j=i}^{n} X_i X_j \tag{28}$$

T a b l e 1 – *Correlations for properties[23]*

Parameter	Correlation
Oil density	$$\rho(P,T) = \rho_0 + \Delta\rho_P - \Delta\rho_T$$ $$\Delta\rho_P = \left[0.167 + \left(16.181 \cdot 10^{-0.0425\rho_0}\right)\right]\left(\frac{P}{1000}\right) - 0.01\left[0.299 + \left(263 \cdot 10^{-0.0603\rho_0}\right)\right]\left(\frac{P}{1000}\right)^2$$ $$\Delta\rho_T = \left[0.0133 + 152.4 \cdot \left(\rho_0 + \Delta\rho_P\right)^{-2.54}\right](T-520) - \left[8.1 \cdot 10^{-6} - 0.0622 \cdot 10^{-0.764(\rho_0+\Delta\rho_P)}\right](T-520)^2$$
Henry coefficient	$$H_i = \frac{\nu_N}{\lambda_i \rho_L}$$
Solubility of H_2	$$\lambda_{H_2} = -0.559729 - \left(0.42947 \cdot 10^{-3}\right)T + 3.07539\left(\frac{T}{\rho_{20}}\right) + \left(1.94593 \cdot 10^{-6}\right)T^2 + \frac{0.835783}{\rho_{20}^2}$$
Solubility of H_2S	$$\lambda_{H_2S} = e^{(3.3670 - 0.008470 \cdot T)}$$
Gas-liquid mass transfer coefficient	$$\frac{k_i^L a_L}{D_i^L} = 7\left(\frac{G_L}{\mu_L}\right)^{0.4}\left(\frac{\mu_L}{\rho_L D_i^L}\right)^{1/2}$$
Dynamic liquid viscosity	$$\mu_L = \left(3.141 \cdot 10^{10}\right)(T-460)^{-3.444}\left[\log_{10}(API)\right]^a$$ $$a = 10.313\left[\log_{10}(t-460)\right] - 36.477$$
Diffusivity	$$D_i^L = \left(8.93 \cdot 10^{-8}\right)\left(\frac{\nu_L^{0.267}}{\nu_i^{0.433}}\right)\left(\frac{T}{\mu_L}\right)$$
Molar volume	$$\nu = 0.285\nu_c^{1.048}$$ $$\nu_c^m = \left(7.5214 \cdot 10^{-3}\right)\left(T_{MeABP}^{0.2896}\right)\left(d_{15.6}^{-0.7666}\right)$$
Liquid-solid mass transfer coefficient	$$\frac{k_i^s}{D_i^L a_s} = 1.8\left(\frac{G_L}{a_s\mu_L}\right)^{1/2}\left(\frac{\mu_L}{\rho_L D_i^L}\right)^{1/3}$$
Specific surface area	$$a_s = \frac{6}{d_p}(1-\varepsilon)$$

Artificial neural networks

ANNs are an excellent tool for fitting functions and recognizing patterns. Simple operational elements work in parallel to form neural networks, inspired by the biological nervous system[33]. Various types of ANNs exist, such as recurrent, radial basis, function networks, and self-organizing maps. However, feed-forward ANNs are most commonly used for fitting and predicting operational functions. These networks comprise one input layer, one or more hidden layers, and one output layer. The neurons in each layer transmit information from the input layer to the hidden layers, and then to the output layer[34]. Independent and response variables have an impact on the number of input and output layer neurons. There is no set rule for the number of neurons in the hidden layers; trial and error is the most common method for determining this[35].

Assuming the hidden layer has the appropriate number of neurons and the hyperbolic tangent sigmoid (tansig) and purelin functions are used as activation functions for the hidden and output layers, respectively, feed-forward ANNs with a hidden layer can predict both linear and nonlinear functions very accurately[33].

Before use, ANNs need to be trained to determine weight and bias values. Various methods exist for training neural networks, with the backpropagation method using the Levenberg-Marquardt (LM) learning rule being one of the most common[36].

In this study, feed-forward ANNs were employed to predict the response variable (outlet sulfur content). The backpropagation approach was used to train the expressed ANNs, utilizing three learning rules: LM, BR, and Scaled Conjugate Gradient (SCG). Training ceases automatically in LM and SCG when generalization stops improving, as indicated by an increase in the mean square error of validation samples. However, in BR, training stops based on adaptive weight minimization (regularization)[37]. Artificial neural networks with 10, 20, or 30 neurons in the hidden layer were built for each type of learning method, and their results were compared.

N-fold cross-validation

Cross-validation is a model evaluation method that examines the generalizability and independence of statistical analysis outcomes from the training data set. *N*-fold cross-validation divides the data into *N* subgroups. In each iteration, one subgroup is used for testing and the other *N*–1 for training. This procedure is repeated *N* times, ensuring all data is used exactly once for training and testing. The average result of these *N*-times is taken as the final estimate of model accuracy. For the ANN with LM and SCG learning methods, three sets of data are used: training, validation, and testing. In these cases, one subset must be allocated to the validation data set in an *N*-fold cross-validation[37]. Appendix *A* illustrates the 5-fold cross-validation method employed in this investigation.

Results and discussion

Reactor simulation

The simulation results were validated using a pilot plant data set for HDS on Kuwaiti atmospheric residues[38]. Table 2 shows the operating conditions for this validation scenario[38].

A comparison between the predicted sulfur weight percent based on the simulation and experimental pilot plant data for different deactivation functions is shown in Fig. 1. Functions ranging from the simplest relationships with time, such as nonlinear and exponential functions (γ_1, γ_2), to more complex relationships with time γ_3, γ_4 and operating temperature (γ_5) were considered. All functions were able to predict the experimental pilot plant data well. As shown in Fig. 1, the exponential deactivation functions (γ_2, γ_4) demonstrated more accurate modeling adaptability compared to nonlinear deactivation functions (γ_1, γ_3), based on their RSME and R^2 results. The simulation with the γ_4 deactivation function was the most accurate, based on its

Table 2 – *Operating conditions for the validation scenario[38]*

Feedstock	
Feed properties	Value
API (°)	12.27
Total sulfur concentration (wt %)	4.30
Asphaltenes concentration (wt %)	3.75
Total nitrogen concentration (wt-ppm)	2670.00
Kinematic viscosity at 50 °C	871.20
Carbon residue (wt %)	12.20
Nickel concentration (wt-ppm)	21.00
Vanadium concentration (wt-ppm)	69.00
Operating conditions	
Temperature (°C)	374.85
Pressure (MPa)	12
u_G (cm s^{-1})	0.75
u_L (cm s^{-1})	$1.31 \cdot 10^{-3}$
Reactor length (cm)	17
LHSV (h^{-1})	0.28
H$_2$ / Oil (std m^3 m^{-3})	570
Catalyst properties	
Equivalent diameter (mm)	2.54
Specific surface area (m^2 g^{-1})	175
Pore volume (cm^3 g^{-1})	0.56
Molybdenum content (wt %)	10.7
Nickel content (wt %)	2.9
Bulk density (g cm^{-3})	0.8163

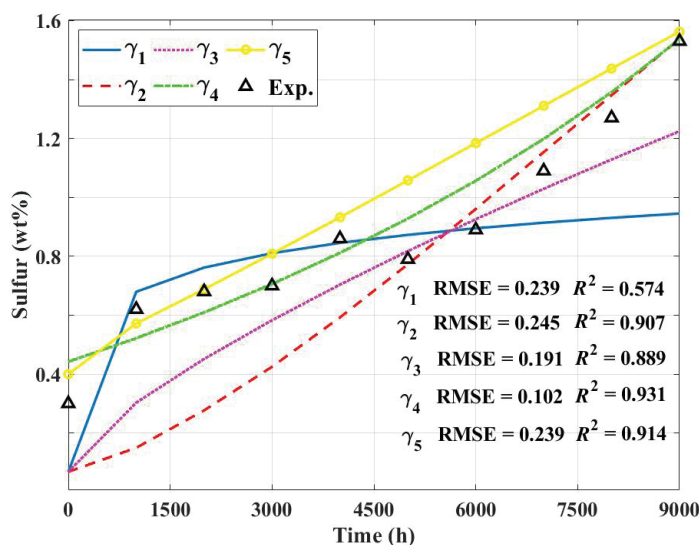|		
γ_1	RMSE = 0.239	$R^2 = 0.574$
γ_2	RMSE = 0.245	$R^2 = 0.907$
γ_3	RMSE = 0.191	$R^2 = 0.889$
γ_4	RMSE = 0.102	$R^2 = 0.931$
γ_5	RMSE = 0.239	$R^2 = 0.914$

F i g . 1 – *Comparison between the predicted sulfur weight percent from simulation and experimental pilot plant data for different deactivation functions*
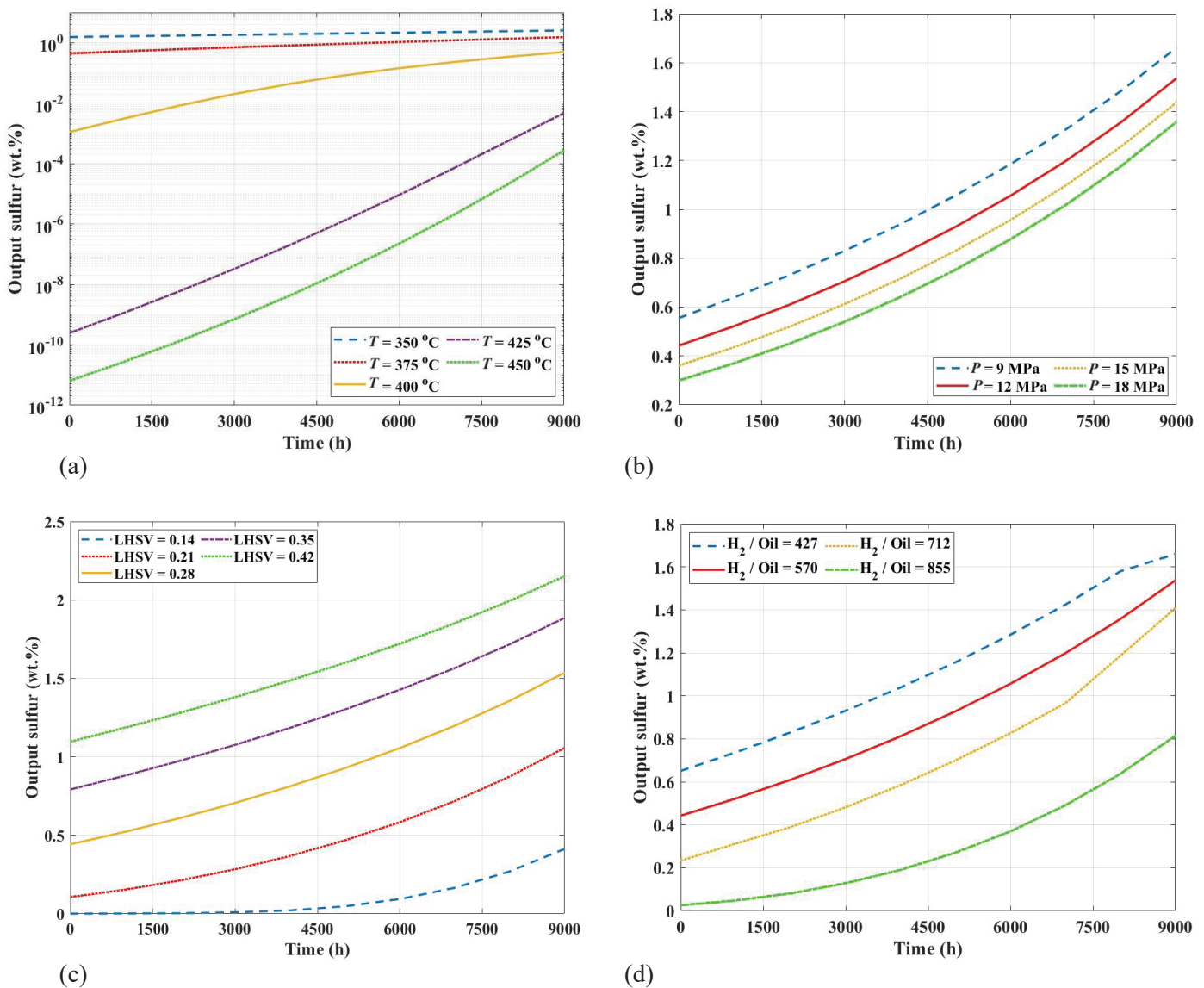
(a)

(b)

(c)

(d)

F i g . 2 – *Effect of (a) temperature, (b) pressure, (c) liquid hourly space velocity (LHSV), and (d) hydrogen to oil ratio on the outlet sulfur concentration*

lowest RMSE and highest R^2 results (RMSE=0.102, R^2=0.931). This accuracy aligns well with the long working time of the catalyst, making it a good result for the impact of time on HDS catalyst deactivation. The steady-state catalyst activity term (φ_s) plays a significant role in this good accuracy. As seen in Fig. 1, the simulation with the γ_5 deactivation function provided accurate predictions for the short working time of the HDS catalyst (less than 4500 h). It can be inferred that temperature significantly affects the early hours of the HDS process, where asphaltene molecules typically convert into coke, which deposits on the catalyst surface. Additionally, it was also observed that the sulfur output concentration increased over time due to coke deposits on the catalyst's surface, causing it to deactivate.

Effect of operating variables on the outlet sulfur content

This section evaluates the sensitivity analysis and the effect of operating variables on the outlet sulfur content (Fig. 2). When examining the impact of each variable, the values of the other variables are constant and equal to those in Table 2.

Fig. 2(a) shows the effect of temperature on output sulfur concentration using the optimal catalyst deactivation function (γ_4) due to its greater accuracy for predicting the pilot plant data compared to other deactivation functions. Increasing the temperature within the studied temperature range enhanced the HDS reaction rate, improved reactor performance, and reduced sulfur output. Fig. 2(b) displays the pressure effect on the outlet sulfur con-

tent with the γ_4 deactivation function. The results indicate that increasing pressure reduced the outlet sulfur concentration, as the HDS reaction rate was inversely related to concentration. Fig. 2(c) illustrates the effect of liquid hourly space velocity (LHSV). Increasing LHSV had an adverse effect on the removal of sulfur, because higher LHSV shortened the residence time of the feed in the reactor, leading to faster catalyst deactivation. Reducing LHSV improved sulfur conversion and prolonged catalyst life. Fig. 2(d) depicts the effect of the hydrogen-to-oil ratio. This ratio had a direct relationship with sulfur removal because the inlet hydrogen flow increased with a higher ratio.

Modeling the simulation results

To reduce the temperature-path optimization time, the results obtained from the HDS reactor simulation were modeled using RSM and ANN methods. The output sulfur was simulated at 250 different temperatures (between 350 and 450 °C) and catalyst operating times (between 0 and 9000 h) using dynamic simulation. This data set, provided in Appendix *B,* was used as input data for the modeling methods. The values of other operational variables, such as pressure, LHSV, and hydrogen-to-oil ratio, were kept constant at their optimal values obtained in the previous section. As mentioned, 5-fold cross-validation was used in all modeling methods of this study (according to Appendix *A*). This strategy divided the data into five subgroups, each containing 50 data points, to enhance model accuracy and independence from the training data. Four subgroups were dedicated to training, and one subgroup to testing for RSM and ANN with the BR learning method. For other methods, three subsets were used for training, one subset for validation, and one subset as a test data set. This process was repeated five times for all modeling methods. All the data was utilized as test data once, and model accuracy was assessed by the model's average performance over these five iterations. Additionally, all modeling methods normalized dependent and independent variables between 0 and 1.

RSM results

Equations (29) to (33) show the RSM curves for the first to fifth iteration in the 5-fold cross-validation method:

Iteration 1: (29)

$$\overline{S} = 0.2273 - 1.4729\overline{T} + 0.5495\overline{t} + 1.4549\overline{T}^2 - 0.0528\overline{t}^2 - 0.6612\overline{t} \cdot \overline{T}$$

Iteration 2: (30)

$$\overline{S} = 0.4097 - 1.8387\overline{T} + 0.2767\overline{t} + 1.6768\overline{T}^2 + 0.0468\overline{t}^2 - 0.4714\overline{t} \cdot \overline{T}$$

Iteration 3: (31)

$$\overline{S} = 0.3922 - 1.8425\overline{T} + 0.5005\overline{t} + 1.6693\overline{T}^2 - 0.1187\overline{t}^2 - 0.5461\overline{t} \cdot \overline{T}$$

Iteration 4: (32)

$$\overline{S} = 0.3685 - 1.6815\overline{T} + 0.3738\overline{t} + 1.5648\overline{T}^2 + 0.1076\overline{t}^2 - 0.6888\overline{t} \cdot \overline{T}$$

Iteration 5: (33)

$$\overline{S} = 0.3597 - 1.7436\overline{T} + 0.3838\overline{t} + 1.6496\overline{T}^2 - 0.0112\overline{t}^2 - 0.5592\overline{t} \cdot \overline{T}$$

Table 3 presents the results of the analysis of variance (ANOVA) for the RSM models. The *F*-values in this table indicate whether the proposed models can adequately describe the dependent variables. The degrees of freedom of the model are derived from the number of variable groups examined. In these models, the right side of the equation includes five groups of variables: normalized temperature, normalized time, normalized temperature squared, normalized time squared, and the product of normalized temperature and time, resulting in the model degrees of freedom of 5. The degrees of freedom

T a b l e 3 – *Results of ANOVA for the RSM models*

| Iteration No.	Source	Degrees of freedom (df)	Sum of squares (SS)	Mean of squares (MS)	F value
1	Regression	5	5.394	1.079	122.5
	Error	194	1.708	0.009	
	Total	199	7.102		
2	Regression	5	6.877	1.375	118.4
	Error	194	2.255	0.012	
	Total	199	9.132		
3	Regression	5	7.807	1.561	148.5
	Error	194	2.040	0.011	
	Total	199	9.847		
4	Regression	5	8.628	1.726	160.6
	Error	194	2.085	0.011	
	Total	199	10.71		
5	Regression	5	5.982	1.196	117.5
	Error	194	1.975	0.010	
	Total	199	7.957		
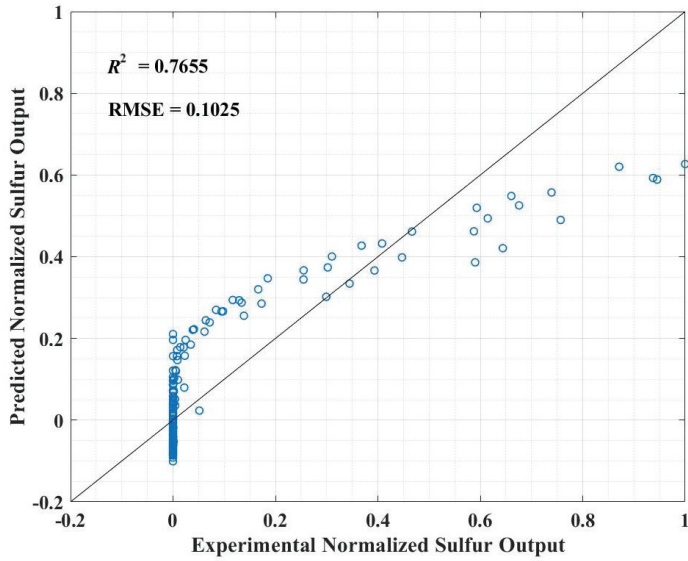
Fig. 3 – *Comparison between simulation and response surface modeling results for dimensionless output sulfur value*

Fig. 4 – *Comparison between the results of the best ANN method and simulation for dimensionless output sulfur value*

for the error were determined by the difference between the number of trained data points and the number of variable groups in the model, minus one. The total degrees of freedom equal the number of training data points minus one. The sum of squares for the model equals the sum of squares of the difference between the model-predicted values and the mean values, while the sum of squares for the error equals the sum of squares of the difference between the model-predicted values and the experimental values. The mean square is obtained by dividing the sum of squares by the degrees of freedom. To calculate the *F*-value, the model's mean square is divided by the error. This value should be compared with the critical value obtained from the distribution

Table 4 – *Coefficient of determination (R^2) and root mean square error (RMSE) values for the response surface models*

Iteration No.	Training data		Test data		Total data	
	R^2	RMSE	R^2	RMSE	R^2	RMSE
1	0.7595	0.0924	0.9136	0.1576	0.7509	0.1086
2	0.7531	0.1062	0.8045	0.0910	0.7621	0.1033
3	0.7929	0.1010	0.7337	0.1184	0.7630	0.1047
4	0.8054	0.1021	0.6603	0.1189	0.7587	0.1057
5	0.7517	0.0994	0.7979	0.1166	0.7640	0.1030

function *F*. Given a confidence level of 0.05 (α = 0.05) and degrees of freedom of 4 and 245 for the model and error, respectively, the critical *F*-value is defined as follows[36,39]:

$$F_{(0.05)}(4,245) = 2.260 \qquad (34)$$

As evident, the *F*-values for the models listed in Table 3 are significantly higher than the critical *F*-value. Therefore, it can be concluded that RSM models are statistically significant, and the relationship between independent and dependent variables is not random[36,37].

The root mean square error (RMSE) and coefficient of determination (R^2) values for the training and test data of the suggested models are calculated and presented in Table 4 to evaluate the accuracy of the RSM in predicting the dependent variable. By averaging equations 24 through 29, the general form of the RSM equation is derived as follows:

$$\overline{S} = 0.3515 - 1.7158\overline{T} + 0.4169\overline{t} + \qquad (35)$$
$$1.6031\overline{T}^2 - 0.0057\overline{t}^2 - 0.5853\overline{t} \cdot \overline{T}$$

Fig. 3 compares the simulation results for dimensionless output sulfur values with the RSM-predicted results. As shown in Fig. 3 and Table 4, the RSM models have too low R^2 values and high RMSE values, indicating poor performance in predicting the reactor output sulfur content. Therefore, the RSM method is unsuitable for this purpose.

ANN results

In this study, three types of feed-forward ANNs with different learning methods (SCG, BR, and LM) were employed to predict the reactor's sulfur output, as previously discussed. The 5-fold cross-validation procedure was also employed to prevent overfitting (see Appendix *A*). The number of neurons in the hidden layer was set to 10, 20, and 30. Table 5 displays the performance of the ANN models. In each model presented, the predicted value was the arithmetic mean of the responses.
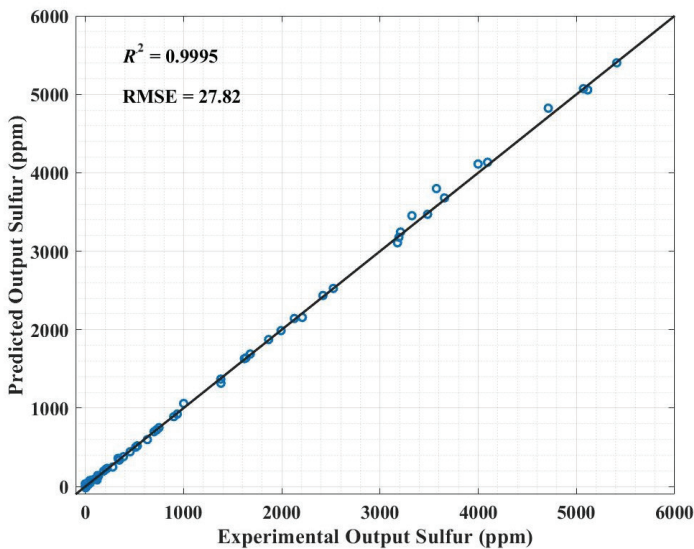
Table 5 – *Coefficient of determination (R^2) and root means square error (RMSE) values for the artificial neural network models*

Learning method	No. of neurons		Training data Iteration's number					Validation data Iteration's number					Test data Iteration's number					Total
			1	2	3	4	5	1	2	3	4	5	1	2	3	4	5	
Levenberg-Marquardt	10	RMSE	22.04	37.89	78.72	54.41	56.07	46.55	84.55	19.21	47.32	37.22	102.0	31.79	54.28	19.62	41.06	48.01
		R^2	0.9997	0.9985	0.9954	0.9981	0.9983	0.9877	0.9968	0.9999	0.9997	0.9988	0.9957	0.9997	0.9996	0.9996	0.9897	0.9982
	20	RMSE	30.42	34.62	69.19	35.81	59.21	31.06	54.57	21.17	73.64	22.44	85.56	37.00	24.78	54.88	24.58	40.27
		R^2	0.9995	0.9986	0.9957	0.9992	0.9982	0.9941	0.9987	0.9998	0.9993	0.9994	0.9968	0.9995	0.9996	0.9973	0.9963	0.9988
	30	RMSE	57.36	42.65	56.05	60.33	47.14	47.18	71.15	23.71	14.75	53.35	74.71	38.01	68.96	16.92	40.11	43.40
		R^2	0.9981	0.9980	0.9973	0.9978	0.9989	0.9864	0.9976	0.9998	0.9999	0.9976	0.9971	0.9995	0.9979	0.9997	0.9904	0.9986
Bayesian Regularization	10	RMSE	13.27	64.58	21.54	98.13	19.83						30.87	35.84	40.73	115.75	14.75	27.82
		R^2	0.9999	0.9950	0.9995	0.9943	0.9998						0.9992	0.9994	0.9992	0.9894	0.9996	0.9995
	20	RMSE	35.82	9.47	61.52	26.54	82.33						50.60	72.12	30.52	66.46	85.45	27.87
		R^2	0.9992	0.9999	0.9962	0.9996	0.9963						0.9978	0.9977	0.9997	0.9967	0.9870	0.9994
	30	RMSE	22.29	138.1	34.10	71.25	38.78						92.53	33.68	30.13	25.87	24.94	31.88
		R^2	0.9997	0.9813	0.9988	0.9970	0.9992						0.9930	0.9995	0.9991	0.9987	0.9989	0.9992
Scaled Conjugate Gradient	10	RMSE	197.0	74.58	92.25	117.9	76.11	138.2	108.6	114.0	65.58	70.54	232.2	67.39	77.28	105.9	64.18	97.30
		R^2	0.9790	0.9945	0.9921	0.9931	0.9971	0.8929	0.9953	0.9972	0.9989	0.9966	0.9793	0.9989	0.9975	0.9972	0.9762	0.9932
	20	RMSE	163.3	567.5	54.87	597.3	251.0	319.1	748.0	57.48	340.0	271.9	226.5	737.7	67.30	477.3	546.2	261.4
		R^2	0.9832	0.6771	0.9972	0.7784	0.9673	0.8593	0.7422	0.9989	0.9289	0.9686	0.9743	0.9464	0.9993	0.8056	0.7981	0.9522
	30	RMSE	214.1	131.2	478.0	239.6	125.2	138.1	118.0	291.9	208.7	100.0	191.4	123.2	466.5	200.6	108.2	155.4
		R^2	0.9697	0.9788	0.7878	0.9665	0.9918	0.8865	0.9928	0.9816	0.9744	0.9904	0.9814	0.9944	0.8883	0.9660	0.9350	0.9830

Among the ANN models, the ANN model using the BR learning method with 10 neurons in the hidden layer performed the best. Fig. 4 compares the output sulfur value from the simulation with the results of this optimal ANN method.

Finding the optimum temperature path

As observed, the feed-forward ANN method with ten neurons in the hidden layer and trained using the BR method outperformed other modeling methods. This method was utilized to plot a three-dimensional curve of sulfur output content versus temperature and catalyst operating time, and subsequently to determine the optimum operating temperature path in terms of catalyst working time, while ensuring the sulfur content in the diesel fuel output from the HDS reactor meets the Euro-6 standard. Fig. 5(a) shows the three-dimensional curve, while Fig. 5(b) presents the contour plot of this curve. It is evident that the catalyst's working time, deactivation, and operating temperature directly influence the sulfur content in the product, corroborating the findings from the previous sections. Assuming a constant sulfur output of 10 ppm (Fig. 5(a)), Fig. 6 depicts the optimal temperature path versus the catalyst working time. This figure illustrates the minimum operating temperature required at each catalyst active time for the diesel-fuel sulfur content to meet the Euro-6 standard, which is less than 10 ppm. Given that the optimal ANN model was used to determine the optimum temperature path and that this model has a low error margin, it is advisable to use an alternative temperature path ensuring the sulfur output is 5 ppm to guarantee compliance with the fuel standard.
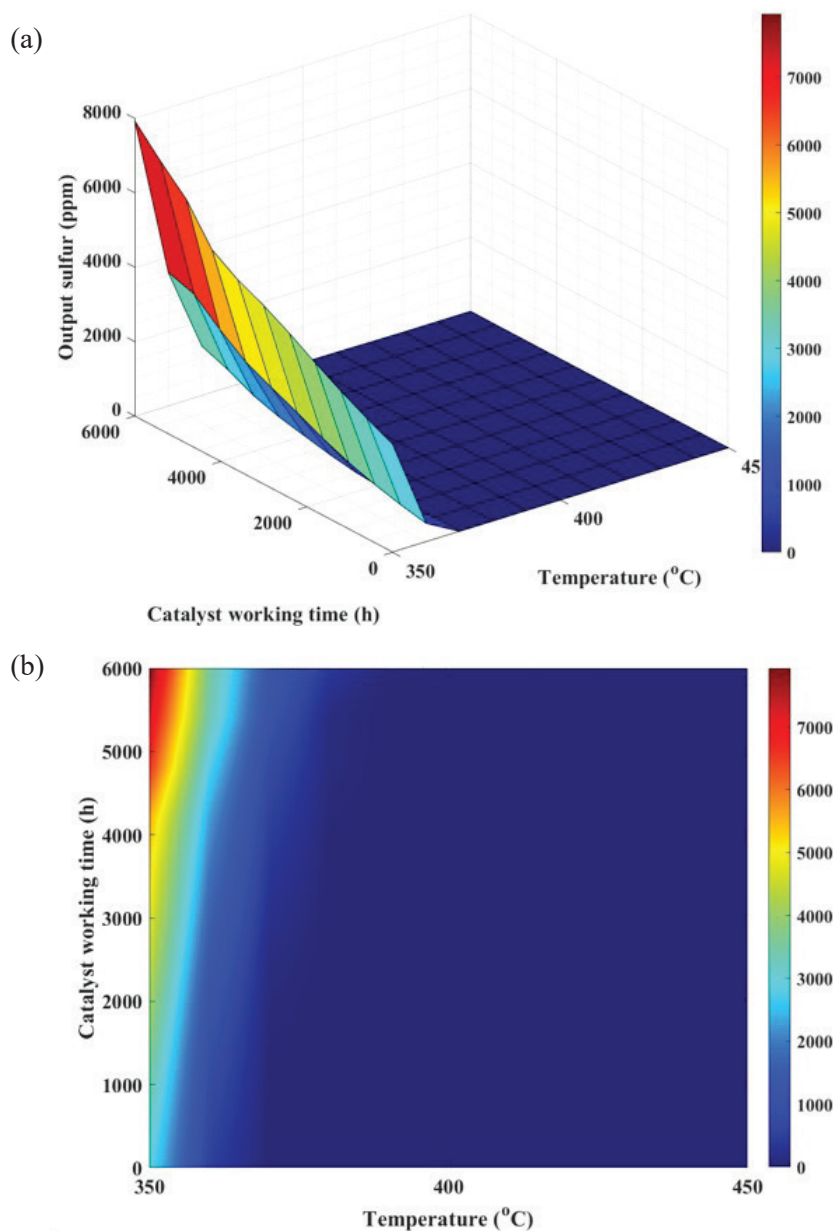
(a)

(b)

Fig. 5 – *Effect of temperature and catalyst working time on output sulfur content (a) 3D, and (b) 2D*
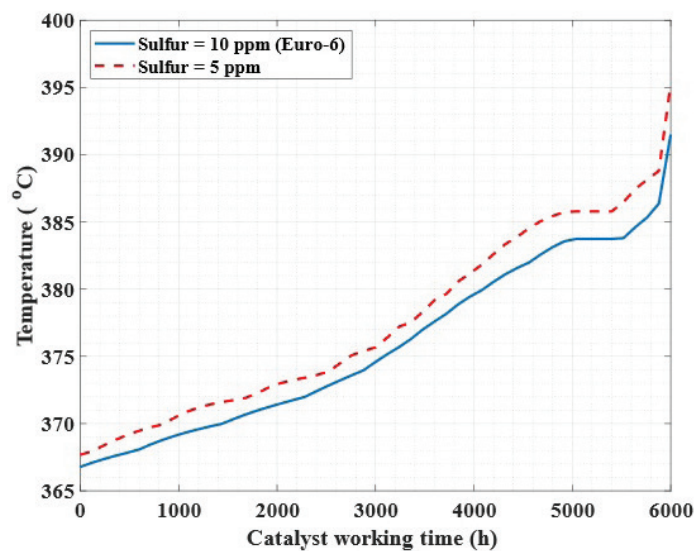

Fig. 6 – *Optimum temperature path versus catalyst working time*

Conclusion

According to the Euro-6 standard, the sulfur content of diesel should be less than 10 ppm. In this study, the optimum temperature path versus the catalyst working time was calculated to ensure the sulfur content in the diesel output of the HDS unit meets the Euro-6 standard. To track the rate of HDS catalyst deactivation, five catalyst deactivation functions (γ_1–γ_5) were assumed. HDS profiles determined with the deactivation model as a function of time (0–9000 h) were compared with experimental data. Among these, γ_4 showed good agreement with real pilot-plant data compared to other functions (R^2 = 0.93, RMSE = 0.102 wt%). The effect of operational variables on the reactor model was then examined using the optimal catalyst deactivation function γ_4. Increasing the temperature (between 350 and 450 °C) had a positive effect on the HDS reaction, reducing the output sulfur concentration. Similarly, higher pressure (between 9 and 18 MPa) and hydrogen-to-oil ratios (between 422 and 855) also reduced the output sulfur concentration. However, increasing LHSV (between 0.14 and 0.42) had a negative effect on the HDS process. To recommend the best HDS operating temperature, the values of the operational variables were kept constant. Given that running the reactor simulation code takes about 15 minutes each time, it was impractical to use it as a fitness function for optimizing the temperature path. Therefore, to reduce optimization time, the RSM and ANN methods were used to model the simulation results. A 5-fold cross-validation procedure was applied to prevent overfitting. The performances of three types of ANN, using LM, BR, and SCG learning methods, were compared. The number of neurons in the hidden layer was set to 10, 20, and 30, respectively. Among these approaches, the feed-forward ANN method with ten neurons in the hidden layer and the BR training rule performed the best. This network was used as an evaluation function to determine the optimum temperature path. A three-dimensional curve of sulfur content in diesel was plotted against temperature and catalyst operating time. From this curve, the optimal temperature path was determined by maintaining the sulfur constant at 10 ppm. This path represents the minimum temperature required during the catalyst's life to ensure the sulfur concentration in the diesel remained below ten ppm, in compliance with the Euro-6 standard. Since simulation and modeling results always have a small error, the optimum temperature path for the output concentration of 5 ppm was also calculated to ensure the quality of the final product.

Nomenclature

A	–	Aromatics
ANN	–	Artificial neural network
API	–	American petroleum institute (API) gravity
a_L	–	Gas-liquid interfacial area, cm^{-1}
a_s	–	Liquid-solid interfacial area, cm^{-1}
BR	–	Bayesian regularization
BVP	–	Boundary value problem
C_i^L	–	Molar concentration of compound i in the liquid phase, mol cm^{-3}
$(C_i^L)_0$	–	Molar concentration of compound i in the liquid phase at the reactor input, mol cm^{-3}
C_i^s	–	Molar concentration of compound i in the solid phase, mol cm^{-3}
D_i^L	–	Molecular diffusivity of compound i in liquid, cm^{-2} mol s^{-1}
df	–	Degree of freedom
d_p	–	Particle diameter, cm
E_a	–	Activation energy, kJ mol^{-1}
GA	–	Genetic algorithm
G_L	–	Liquid superficial mass velocity, g cm^{-2} s^{-1}
HDT	–	Hydrotreating
HDS	–	Hydrodesulfurization
HAD	–	Hydrodearomatization
HDN	–	Hydrodenitrogenation
HDM	–	Hydrodemetallation
H_i	–	Henry's law coefficient of compound i, MPa cm^{-3} mol^{-1}
H_2	–	Hydrogen
H_2S	–	Hydrogen sulfide
IVP	–	Initial value problem
k_0	–	Pre-exponential factor
k_i^G	–	Mass transfer coefficient of compound i in the gas phase j, cm s^{-1}
k_i^L	–	Mass transfer coefficient of compound i in the liquid phase j, cm s^{-1}
k_i^s	–	Mass transfer coefficient of compound i in the solid phase j, cm s^{-1}
LHSV	–	Liquid hourly space velocity, h^{-1}
LM	–	Levenberg-Marquardt
MS	–	Means of squares
N	–	Data subgroup number
NSGA-II	–	Non-dominated sorting genetic algorithm-II
N_B	–	Basic nitrogen
N_{NB}	–	Non-basic nitrogen
ODE	–	Ordinary differential equation
P	–	Pressure, kPa
p_i^G	–	Partial pressure of compound i in the gas phase, MPa
$p_{H_2}^G$	–	Partial pressure of hydrogen in the gas phase, MPa

$(p_{H_2}^G)_0$ – Partial pressure of hydrogen in the gas phase at the reactor input, MPa

$p_{H_2S}^G$ – Partial pressure of hydrogen sulfide in the gas phase, MPa

R – Universal gas constant, J mol^{-1} K^{-1}

r – Radius of catalyst, cm

RMSE – Root mean square error

RSM – Response surface method

R^2 – Coefficient of determination

R_p – Radius of catalyst pellet, cm

r_j – Rate of reaction j, mol kg^{-1} s^{-1}

$r_{j,act}$ – Actual rate of reaction j, mol kg^{-1} s^{-1}

$r_{j,surface}$ – Rate of reaction j at the catalyst's surface, mol kg^{-1} s^{-1}

S – Sulfur

$\bar{S}$ – Normalized output sulfur

SCG – Scaled Conjugate Gradient

SS – Sum of squares

T – Temperature, °C

$\bar{T}$ – Normalized temperature

t – Time, h

$\bar{t}$ – Normalized time

TANSIG – Hyperbolic tangent sigmoid

TBR – Trickle-bed reactor

T_0 – Feed temperature, °C

T_{MeABP} – Mean average boiling point, K

t_∞ – Catalyst lifetime, h

u_G – Superficial velocity of the gas phase, cm s^{-1}

u_L – Superficial velocity of the liquid phase, cm s^{-1}

X – Independent variable

Y – Response variable

z – Reactor length, cm

Greek symbols

α_i – Constant deactivation function coefficient, $i = 1, 2, 3$ and 4

γ_k – Catalyst deactivation function, $k = 1, 2, 3, 4$ and 5

ε – Porosity factor

η_j – Catalyst effectiveness factor

λ_i – Solubility coefficient of compound i, mol L^{-1}

v_c – Critical specific volume of the gaseous compounds, cm^3 mol^{-1}

v_i – Molar volume of the solute i at normal boiling temperature, cm^3 mol^{-1}

v_{Li} – Molar volume of the solvent i at normal boiling temperature, cm^3 mol^{-1}

v_N – Molar gas volume at standard conditions (15.6 °C and 101.3 kPa), cm^3 mol^{-1}

v_c^m – Critical specific volume, m^3 kg^{-1}

μ_L – Liquid viscosity, mPa s

ρ_B – Catalyst bulk density, kg m^{-3}

ρ_L – Liquid phase density, g cm^{-3}

$\rho(P, T)$ – Liquid density at P kPa and T °C, kg m^{-3}

ρ_0 – Liquid density at standard conditions (15.6 °C and 101.3 kPa), kg m^{-3}

ρ_{20} – Liquid density at 20 °C, g cm^{-3}

φ_s – Steady state catalyst activity

Subscripts

G – Gas phase

i – Compound (H$_2$, H$_2$S, non-basic nitrogen, basic nitrogen, aromatic, sulfur)

j – Reaction (HDS, HDA, HDA$_{NB}$, HDAN$_B$)

L – Liquid phase

0 – Reactor inlet condition

Superscript

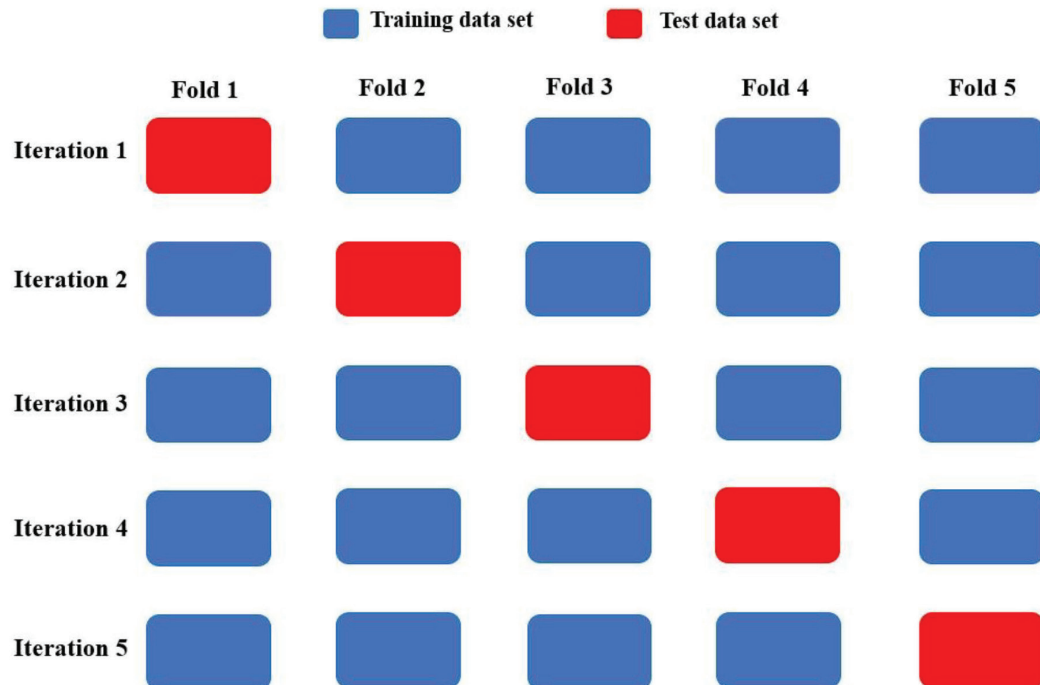G – Gas phase

L – Liquid phase

S – Solid phase

STATEMENTS AND DECLARATIONS

A p p e n d i x   A .

Diagram of 5-fold cross-validation for (a) RSM and ANN with BR learning method, and (b) ANN with LM and SCG learning methods

(a)

(b)

A p p e n d i x   *B* .

Input data of the modeling methods

Temperature (°C)	Time (h)	Output sulfur (ppm)	Temperature (°C)	Time (h)	Output sulfur (ppm)
400	1500	$1.58 \cdot 10^{-6}$	415	500	$1.09 \cdot 10^{-9}$
410	0	$8.36 \cdot 10^{-10}$	400	2000	$1.20 \cdot 10^{-5}$
430	500	$6.98 \cdot 10^{-7}$	350	4000	$5.41 \cdot 10^{3}$
405	1000	$4.80 \cdot 10^{-9}$	405	2500	$5.62 \cdot 10^{-6}$
350	500	$3.19 \cdot 10^{3}$	355	500	$1.62 \cdot 10^{3}$
395	500	$1.26 \cdot 10^{-6}$	415	500	$1.09 \cdot 10^{-9}$
395	500	$1.26 \cdot 10^{-6}$	410	2000	$2.45 \cdot 10^{-8}$
445	500	$2.05 \cdot 10^{-9}$	355	1000	$1.87 \cdot 10^{3}$
410	0	$8.36 \cdot 10^{-10}$	355	1500	$2.13 \cdot 10^{3}$
420	0	$1.41 \cdot 10^{-9}$	355	3500	$3.32 \cdot 10^{3}$
420	1000	$1.42 \cdot 10^{-9}$	355	4000	$3.66 \cdot 10^{3}$
385	500	$1.90 \cdot 10^{-3}$	395	2500	$1.30 \cdot 10^{-3}$
400	2000	$1.20 \cdot 10^{-5}$	435	2500	$2.35 \cdot 10^{-9}$
405	1500	$5.10 \cdot 10^{-8}$	410	2500	$3.66 \cdot 10^{-7}$
350	1000	$3.48 \cdot 10^{3}$	400	2500	$8.72 \cdot 10^{-5}$
405	2000	$5.48 \cdot 10^{-7}$	435	3000	$2.38 \cdot 10^{-9}$
420	1500	$1.43 \cdot 10^{-9}$	355	4000	$3.66 \cdot 10^{3}$
395	1500	$4.00 \cdot 10^{-5}$	440	0	$2.66 \cdot 10^{-9}$
435	1000	$8.54 \cdot 10^{-7}$	355	4500	$4.00 \cdot 10^{3}$
425	500	$1.88 \cdot 10^{-9}$	400	2500	$8.72 \cdot 10^{-5}$
385	500	$1.90 \cdot 10^{-3}$	355	5500	$4.71 \cdot 10^{3}$
395	1500	$4.00 \cdot 10^{-5}$	405	2500	$5.62 \cdot 10^{-6}$
390	1500	$1.13 \cdot 10^{-3}$	360	1000	$7.49 \cdot 10^{2}$
430	4000	$1.38 \cdot 10^{-5}$	425	1000	$1.86 \cdot 10^{-9}$
425	500	$1.88 \cdot 10^{-9}$	435	3000	$2.38 \cdot 10^{-9}$
395	2000	$2.47 \cdot 10^{-4}$	440	500	$2.18 \cdot 10^{-9}$
420	1500	$1.43 \cdot 10^{-9}$	450	5500	$1.19 \cdot 10^{2}$
445	3000	$1.77 \cdot 10^{-9}$	400	2500	$8.72 \cdot 10^{-5}$
430	4000	$1.38 \cdot 10^{-5}$	375	1000	$2.22 \cdot 10^{0}$
420	2000	$1.43 \cdot 10^{-9}$	360	1000	$7.49 \cdot 10^{2}$
350	1000	$3.48 \cdot 10^{3}$	400	3500	$3.70 \cdot 10^{-3}$
390	2000	$4.60 \cdot 10^{-3}$	410	2500	$3.66 \cdot 10^{-7}$
410	1500	$1.87 \cdot 10^{-9}$	425	2500	$1.88 \cdot 10^{-9}$
395	2000	$2.47 \cdot 10^{-4}$	360	1500	$9.35 \cdot 10^{2}$
350	2000	$4.09 \cdot 10^{+3}$	415	1000	$1.09 \cdot 10^{-9}$
375	500	$9.75 \cdot 10^{-1}$	400	3500	$3.72 \cdot 10^{-3}$
435	1500	$2.35 \cdot 10^{-9}$	360	1500	$9.35 \cdot 10^{2}$
350	2000	$4.09 \cdot 10^{3}$	445	3500	$1.10 \cdot 10^{-7}$
435	2500	$2.35 \cdot 10^{-9}$	410	4500	$7.50 \cdot 10^{-3}$
350	3500	$5.07 \cdot 10^{3}$	395	3000	$6.52 \cdot 10^{-3}$

Temperature (°C)	Time (h)	Output sulfur (ppm)	Temperature (°C)	Time (h)	Output sulfur (ppm)
445	3500	$1.10 \cdot 10^{-7}$	440	500	$2.18 \cdot 10^{-9}$
415	1500	$1.09 \cdot 10^{-9}$	445	3500	$1.10 \cdot 10^{-7}$
395	3500	$3.04 \cdot 10^{-2}$	365	2500	$5.28 \cdot 10^{2}$
435	4500	$1.06 \cdot 10^{-3}$	400	4000	$2.15 \cdot 10^{-2}$
405	2500	$5.62 \cdot 10^{-6}$	390	5000	$7.73 \cdot 10^{0}$
405	3000	$5.39 \cdot 10^{-5}$	400	5000	$5.38 \cdot 10^{-1}$
420	2500	$2.56 \cdot 10^{-9}$	375	3500	$7.63 \cdot 10^{1}$
385	1000	$6.59 \cdot 10^{-3}$	365	3000	$6.99 \cdot 10^{2}$
375	1500	$4.89 \cdot 10^{0}$	395	5000	$1.96 \cdot 10^{0}$
410	5000	$6.39 \cdot 10^{-2}$	365	3000	$6.99 \cdot 10^{2}$
435	4500	$1.06 \cdot 10^{-3}$	365	3500	$9.00 \cdot 10^{2}$
390	2000	$4.60 \cdot 10^{-3}$	445	4000	$4.81 \cdot 10^{-5}$
360	1500	$9.35 \cdot 10^{2}$	395	5000	$1.96 \cdot 10^{0}$
395	4000	$1.32 \cdot 10^{-1}$	445	5000	$7.50 \cdot 10^{-1}$
380	500	$4.92 \cdot 10^{-2}$	425	2500	$1.88 \cdot 10^{-9}$
390	3000	$6.91 \cdot 10^{-2}$	365	3500	$9.00 \cdot 10^{2}$
435	4500	$1.06 \cdot 10^{-3}$	420	3500	$2.09 \cdot 10^{-6}$
390	3500	$2.48 \cdot 10^{-1}$	420	3500	$2.09 \cdot 10^{-6}$
390	4000	$8.34 \cdot 10^{-1}$	415	3500	$1.07 \cdot 10^{-5}$
385	2000	$7.26 \cdot 10^{-2}$	405	3500	$4.74 \cdot 10^{-4}$
360	2500	$1.38 \cdot 10^{3}$	365	5000	$1.68 \cdot 10^{3}$
375	3000	$4.12 \cdot 10^{1}$	425	3500	$5.33 \cdot 10^{-7}$
360	3000	$1.63 \cdot 10^{3}$	375	4500	$2.21 \cdot 10^{2}$
395	4500	$5.30 \cdot 10^{-1}$	385	3000	$6.75 \cdot 10^{-1}$
375	3000	$4.12 \cdot 10^{1}$	440	2500	$1.78 \cdot 10^{-9}$
380	1500	$3.72 \cdot 10^{-1}$	435	5000	$5.21 \cdot 10^{-2}$
390	4500	$2.63 \cdot 10^{0}$	390	5000	$7.73 \cdot 10^{0}$
360	4000	$2.21 \cdot 10^{3}$	380	1500	$3.72 \cdot 10^{-1}$
400	4000	$2.15 \cdot 10^{-2}$	410	5500	$4.62 \cdot 10^{-1}$
420	2500	$2.56 \cdot 10^{-9}$	440	3500	$8.00 \cdot 10^{-8}$
375	3000	$4.12 \cdot 10^{1}$	440	4500	$2.48 \cdot 10^{-3}$
430	4500	$7.22 \cdot 10^{-4}$	410	5500	$4.62 \cdot 10^{-1}$
360	4500	$2.52 \cdot 10^{3}$	385	3000	$6.75 \cdot 10^{-1}$
390	5000	$7.73 \cdot 10^{0}$	435	5500	$1.46 \cdot 10^{0}$
360	4500	$2.52 \cdot 10^{3}$	395	5500	$6.63 \cdot 10^{0}$
360	5500	$3.21 \cdot 10^{3}$	440	5000	$1.63 \cdot 10^{-1}$
360	6000	$3.57 \cdot 10^{3}$	365	5500	$1.99 \cdot 10^{3}$
365	500	$1.24 \cdot 10^{2}$	405	3500	$4.74 \cdot 10^{-4}$
365	1000	$1.88 \cdot 10^{2}$	420	4500	$1.19 \cdot 10^{-3}$
375	3500	$7.63 \cdot 10^{1}$	370	0	$7.17 \cdot 10^{0}$
365	1000	$1.88 \cdot 10^{2}$	385	4000	$5.47 \cdot 10^{-4}$
365	2000	$3.87 \cdot 10^{2}$	370	0	$7.17 \cdot 10^{0}$
410	5500	$4.62 \cdot 10^{-1}$	380	3000	$5.83 \cdot 10^{0}$

Temperature (°C)	Time (h)	Output sulfur (ppm)	Temperature (°C)	Time (h)	Output sulfur (ppm)
390	6000	$5.19 \cdot 10^1$	420	6000	$1.43 \cdot 10^{-9}$
405	4500	$2.68 \cdot 10^{-2}$	365	1000	$1.88 \cdot 10^2$
370	1000	$2.59 \cdot 10^1$	415	0	$1.09 \cdot 10^{-9}$
405	6000	$4.45 \cdot 10^0$	400	3500	$3.72 \cdot 10^{-3}$
375	5000	$3.46 \cdot 10^2$	445	5500	$2.38 \cdot 10^1$
375	5500	$5.12 \cdot 10^2$	415	4000	$1.09 \cdot 10^{-9}$
375	6000	$7.25 \cdot 10^2$	430	1000	$1.11 \cdot 10^{-8}$
370	1000	$2.59 \cdot 10^1$	395	2000	$2.47 \cdot 10^{-4}$
445	5500	$2.38 \cdot 10^1$	395	3000	$6.52 \cdot 10^{-3}$
445	6000	$2.79 \cdot 10^2$	435	6000	$2.35 \cdot 10^{-9}$
430	6000	$8.11 \cdot 10^0$	360	1000	$7.49 \cdot 10^2$
425	4000	$2.30 \cdot 10^{-5}$	365	5000	$1.68 \cdot 10^3$
370	1500	$4.66 \cdot 10^1$	365	4000	$1.00 \cdot 10^3$
385	4500	$1.30 \cdot 10^1$	390	2500	$5.83 \cdot 10^{-4}$
370	2500	$1.33 \cdot 10^2$	435	1000	$8.54 \cdot 10^{-7}$
370	3000	$2.09 \cdot 10^2$	430	2500	$1.61 \cdot 10^{-7}$
380	5000	$1.13 \cdot 10^2$	355	3000	$3.18 \cdot 10^3$
420	4500	$1.19 \cdot 10^{-3}$	390	500	$1.11 \cdot 10^{-4}$
415	5000	$3.09 \cdot 10^{-2}$	405	3500	$4.74 \cdot 10^{-4}$
405	6000	$4.45 \cdot 10^0$	390	1500	$1.13 \cdot 10^{-3}$
395	6000	$2.03 \cdot 10^1$	415	2500	$1.09 \cdot 10^{-9}$
380	6000	$3.33 \cdot 10^2$	415	3500	$1.07 \cdot 10^{-5}$
400	5000	$5.38 \cdot 10^{-1}$	380	1500	$3.72 \cdot 10^{-1}$
425	4500	$7.64 \cdot 10^{-4}$	395	1500	$4.00 \cdot 10^{-5}$
425	5000	$1.86 \cdot 10^{-2}$	350	3500	$5.07 \cdot 10^3$
410	6000	$2.80 \cdot 10^0$	450	1500	$2.09 \cdot 10^{-5}$
425	6000	$3.87 \cdot 10^0$	365	5000	$1.68 \cdot 10^3$
415	6000	$2.30 \cdot 10^0$	360	6000	$3.57 \cdot 10^3$
370	4000	$4.55 \cdot 10^2$	385	4500	$1.30 \cdot 10^1$
400	5500	$2.30 \cdot 10^0$	370	2000	$4.51 \cdot 10^1$
385	5000	$3.07 \cdot 10^1$	400	3500	$3.72 \cdot 10^{-3}$
370	4500	$6.31 \cdot 10^2$	385	500	$1.90 \cdot 10^{-3}$
370	6000	$1.38 \cdot 10^3$	445	5500	$2.38 \cdot 10^1$
370	6000	$1.38 \cdot 10^3$	440	5500	$3.27 \cdot 10^{-8}$
355	2000	$2.42 \cdot 10^3$	355	5000	$5.11 \cdot 10^3$
420	4000	$1.43 \cdot 10^{-9}$	425	1500	$1.88 \cdot 10^{-9}$
355	4000	$3.66 \cdot 10^3$	375	3500	$7.63 \cdot 10^1$
355	3000	$3.18 \cdot 10^3$	390	0	$1.10 \cdot 10^{-4}$
400	4000	$2.15 \cdot 10^{-2}$	405	2500	$5.62 \cdot 10^{-6}$
360	4000	$2.21 \cdot 10^3$	445	2000	$4.52 \cdot 10^{-2}$
430	1000	$1.11 \cdot 10^{-8}$	390	1000	$1.17 \cdot 10^{-4}$
430	1000	$1.11 \cdot 10^{-8}$	450	1000	$1.30 \cdot 10^{-6}$

References

1. *Carmona, H. D. P., Akhmetzyanova, U., Tišler, Z., Von-drova, P.,* Hydrotreating atmospheric gasoil and co-process-ing with rapeseed oil using supported Ni-Mo and Co-Mo carbide catalysts, Fuel **268** (2020) 117363.
doi: https://doi.org/10.1016/j.fuel.2020.117363

2. *Mederos, F. S., Ancheyta, J., Elizalde, I.,* Dynamic model-ing and simulation of hydrotreating of gas oil obtained from heavy crude oil, Appl Catal A: Gen. **425** (2012) 13.
doi: https://doi.org/10.1016/j.apcata.2012.02.034

3. *Azarpour, A., Zendehboudi, S.,* A dynamic heterogeneous dispersion model evaluates the performance of industrial catalytic hydrotreating systems, Ind. Eng. Chem. Res. **57** (2018) 8267.
doi: https://doi.org/10.1021/acs.iecr.8b01135

4. *Koh, J. H., Lee, J. J., Kim, H., Cho, A., Moon S. H.,* Cor-relation of the deactivation of CoMo/Al$_2$O$_3$ in hydrodesul-furization with surface carbon species, Appl. Catal. B: Environ. **86** (2009) 176.
doi: https://doi.org/10.1016/j.apcatb.2008.08.002

5. *Mahinsa, P., Sadeghi, M. T., Ganji, H., Shokri, S.,* Two Dimensional dynamic modeling of hydrodesulphurization reactor, J. Petrol Sci. Res. **1** (2012) 32.

6. *Jiang, L., Weng, Y., Liu, C.,* Hydrotreating residue deactiva-tion kinetics and metal deposition, Energ Fuel. **24** (2010) 1475.
doi: https://doi.org/10.1021/ef9014586

7. *Garcia-Martinez, J. C., Chavez-Esquivel, G., Colin-Luna, J. A., de los Reyes-Heredia, J. A.,* Hydrodesulfurization of 4,6–dimethyldibenzothiophene on NiMoP/γ–Al$_2$O$_3$ catalyst under reactive distillation conditions in a micro trickle bed reactor: Solvent and temperature effect, Int. J. Chem. Reac-tor Eng. **21** (2023) 413.
doi: https://doi.org/10.1515/ijcre-2022-0005

8. *Garcia-Martinez, J. C., Dutta, A., Chavez-Esquivel, G., de los Reyes-Heredia, J. A., Castillo-Araiza, C. O.,* Hydrode-sulfurization of dibenzothiophene in a micro trickle bed catalytic reactor under operating conditions from reactive distillation, Int. J. Chem. Reactor Eng. **14** (2016) 769.
doi: https://doi.org/10.1515/ijcre-2015-0126

9. *Chao, Y. C., Chang, J. S., Huang, H. P.,* Dynamic simula-tion of residue hydrodesulfurization trickle-bed reactor, In: Dynamics and Control of Chemical Reactors and Distilla-tion Columns, Elsevier, Bournemouth, 1988, pp 81-86.
doi: https://doi.org/10.1016/B978-0-08-034917-6.50016-7

10. *Rodríguez, E., Felix, G., Ancheyta, J., Trejo, F.,* Modeling of hydrotreating catalyst deactivation for heavy oil hydro-carbons, Fuel **225** (2018) 118.
doi: https://doi.org/10.1016/j.fuel.2018.02.085

11. *Morales–Leal, F. J., Ancheyta, J., Torres–Mancera, P., Alonso, F.,* Experimental methodologies to perform acceler-ated deactivation studies of hydrotreating catalysts, Fuel **332** (2023) 126074.
doi: https://doi.org/10.1016/j.fuel.2022.126074

12. *Torres-Mancera, P., Ancheyta, J., Martínez, J.,* Deactiva-tion of a hydrotreating catalyst in a bench-scale continuous stirred tank reactor at different operating conditions, Fuel **234** (2018) 326.
doi: https://doi.org/10.1016/j.fuel.2018.06.122

13. *Marafi, A., Hauser, A., Stanislaus A.,* Deactivation patterns of Mo/Al$_2$O$_3$, Ni–Mo/Al$_2$O$_3$ and Ni–MoP/Al$_2$O$_3$ catalysts in atmospheric residue hydrodesulphurization, Catal. Today **125** (2007) 192.
doi: https://doi.org/10.1016/j.cattod.2007.03.060

14. *Soltanali, S., Mashayekhi, M., Mohaddecy, S. R. S.,* Com-prehensive investigation of the effect of adding phosphorus and/or boron to NiMo/γ-Al$_2$O$_3$ catalyst in diesel fuel hydro-treating, Process Saf. Environ. **137** (2020) 273.
doi: https://doi.org/10.1016/j.psep.2020.02.033

15. *da Rocha Novaes, L., Secchi, A. R., Salim, V. M. M., de Resende, N. S.,* Enhancement of hydrotreating process eval-uation: Correlation between feedstock properties, in-line monitoring and catalyst deactivation, Catal. Today **394** (2022) 390.
doi: https://doi.org/10.1016/j.cattod.2021.07.026

16. *Tirado, A., Trejo, F., Ancheyta, J.,* Simulation of bench-scale hydrotreating of vegetable oil reactor under non-iso-thermal conditions, Fuel **275** (2020) 117960.
doi: https://doi.org/10.1016/j.fuel.2020.117960

17. *Neto, A. T. P., Fernandes, T. C. R. L., Junior, H. B. d. S., Araujo, A. C. B. d., Alves, J. J. N.,* Three-phase trickle-bed reactor model for industrial hydrotreating processes: CFD and experimental verification, Fuel Process Technol. **208** (2020) 106496.
doi: https://doi.org/10.1016/j.fuproc.2020.106496

18. *Al-Jamimi, H. A., BinMakhasen, G. M., Deb, K., Saleh, T. A.,* Multiobjective optimization and analysis of petroleum refinery catalytic processes: A review, Fuel **288** (2021) 119678.
doi: https://doi.org/10.1016/j.fuel.2020.119678

19. *Srinivas, B., Karthik, S., Sankararao, B.,* Optimization of trickle-bed reactors (TBRs) for hydrodesulfurization (HDS) and hydrodearomatization (HDA) of diesel using single and multiple objectives, Chem. Prod. Process Model. **8** (2013) 93.
doi: https://doi.org/10.1515/cppm-2013-0023

20. *Xie, Y., Posada, F., Minjares, R.,* Diesel sulfur content impacts on Euro VI soot-free vehicles: Considerations for emerging markets. International Council to Clean Transpor-tation (Working Paper) 2020 (2020-11).

21. *Plazas-González, M., Guerrero-Fajardo, C. A., Sodré, J. R.,* Modelling and simulation of hydrotreating of palm oil com-ponents to obtain green diesel, J. Clean. Prod. **184** (2018) 301.
doi: https://doi.org/10.1016/j.jclepro.2018.02.275

22. *Bakhshi Ani, A., Ale Ebrahim, H., Azarhoosh, M. J.,* Simu-lation and multi-objective optimization of a trickle-bed reactor for diesel hydrotreating by a heterogeneous model using non-dominated sorting genetic algorithm II, Energ. Fuel. **29** (2015) 3041.
doi: https://doi.org/10.1021/acs.energyfuels.5b00467

23. *Korsten, H., Hoffmann, U.,* Three-phase reactor model for hydrotreating in pilot trickle-bed reactors, AIChE J. **42** (1996) 1350.
doi: https://doi.org/10.1002/aic.690420515

24. *Azarhoosh, M. J., Ale Ebrahim, H., Pourtarah, S. H.,* Sim-ulating and optimizing hydrogen production by low-pres-sure autothermal reforming of natural gas using non-domi-nated sorting genetic algorithm-II, Chem. Biochem. Eng. Q. **29** (2015) 519.
doi: https://doi.org/10.15255/CABEQ.2014.2158

25. *Froment, G. F., Bischoff, K. B., De Wilde, J.,* Chemical Reactor Analysis and Design. Vol. 2., Wiley, New York, 1990.

26. *Voorhies, Jr. A.,* Carbon formation in catalytic cracking, Ind. Eng. Chem. **37** (1945) 318.
doi: https://doi.org/10.1021/ie50424a010

27. *Rashidzadeh, M., Ahmad, A., Sadighi, S.,* Studying of cata-lyst deactivation in a commercial hydrocracking process (ISOMAX), J. Petrol. Sci. Technol. **1** (2010) 46.
doi: https://doi.org/10.22078/JPST.2010.26

28. *Skala, D. U., Saban, M. D., Orlovic, A. M., Meyn, V. W., Severin, D. K., Rahimian, I. G. H., Marjanovic, M. V.,* Hydrotreating of used oil: Prediction of industrial trickle-bed operation from pilot-plant data, Ind. Eng. Chem. Res. **30** (1991) 2059.
doi: https://doi.org/10.1021/ie00057a002

29. *Elizalde, I., Ancheyta, J.,* Modeling catalyst deactivation during hydrocracking of atmospheric residue by using the continuous kinetic lumping model, Fuel Process. Technol. **123** (2014) 114.
doi: https://doi.org/10.1016/j.fuproc.2014.02.006

30. *Elizalde, I., Ancheyta, J.,* Application of a three-stage approach for modeling the complete period of catalyst deactivation during hydrotreating of heavy oil, Fuel **138** (2014) 45.
doi: https://doi.org/10.1016/j.fuel.2014.02.073

31. *Dean, A., Voss, D., Draguljić, D.,* Response Surface Methodology, in Design and Analysis of Experiments, Springer, 2017, pp 565-614.

32. *Kiadehi, A. D., Taghizadeh, M., Azarhoosh, M. J., Agheinejad-Meybodi, A.,* Hydrogen production using ethylene glycol steam reforming in a micro-reformer: Experimental analysis, multivariate polynomial regression and genetic programming modeling approaches, J. Taiwan Inst. Chem. E. **112** (2020) 20.
doi: https://doi.org/10.1016/j.jtice.2020.07.012

33. *Azarhoosh, M. J., Halladj, R., Askari, S.,* Application of evolutionary algorithms for modelling and optimisation of ultrasound-related parameters on synthesised SAPO-34 catalysts: Crystallinity and particle size, Prog. React. Kinet. Mec. **43** (2018) 236.
doi: https://doi.org/10.3184/146867818X15233705894446

34. *Lotfi, N., Ale Ebrahim, H., Azarhoosh, M. J.,* Proposing a novel theoretical optimized model for the combined dry and steam reforming of methane in the packed-bed reactors, Chem. Pap. **73** (2019) 2309.
doi: https://doi.org/10.1007/s11696-019-00782-1

35. *Azarhoosh, M. J., Halladj, R., Askari, S., Aghaeinejad-Meybodi, A.,* Performance analysis of ultrasound-assisted synthesized nano-hierarchical SAPO-34 catalyst in the methanol-to-lights-olefins process via artificial intelligence methods, Ultrason. Sonochem. **58** (2019) 104646.
doi: https://doi.org/10.1016/j.ultsonch.2019.104646

36. *Maleki-Kakelar, M., Aghaeinejad-Meybodi, A., Sanjideh, S., Azarhoosh, M. J.,* Cost-Effective optimization of bacterial urease activity using a hybrid method based on response surface methodology and artificial neural networks, Environ. Process. **9** (2022) 1.
doi: https://doi.org/10.1007/s40710-022-00564-0

37. *Askari, S., Halladj, R., Azarhoosh, M. J.,* Modeling and optimization of catalytic performance of SAPO-34 nanocatalysts synthesized sonochemically using a new hybrid of non-dominated sorting genetic algorithm-II based artificial neural networks (NSGA-II-ANNs), RSC Adv. **5** (2015) 52788.
doi: https://doi.org/10.1039/C5RA03764F

38. *Kam, E. K. T., Al-Shamali, M., Juraidan, M., Qabazard, H.,* A hydroprocessing multicatalyst deactivation and reactor performance model– pilot-plant life test applications, Energ. Fuel **19** (2005) 753.
doi: https://doi.org/10.1021/ef049843s

39. *Maleki-Kakelar, M., Azarhoosh, M. J., Golmohammadi Senji, S., Aghaeinejad-Meybodi, A.,* Urease production using corn steep liquor as a low-cost nutrient source by *Sporosarcina pasteurii*: Biocementation and process optimization via artificial intelligence approaches, Environ. Sci. Pollut. R. **29** (2022) 13767.
doi: https://doi.org/10.1007/s11356-021-16568-6